PHYSICAL REVIEW B VOLUME 54, NUMBER 11 15 SEPTEMBER 1996-I

Picosecond and millisecond dynamics of photoexcited carriers in porous silicon

P. Malý, F. Trojánek, and J. Kudrna
Faculty of Mathematics and Physics, Charles University, Prague, Czech Republic

A. Hospodková
Institute of Physics, Czech Academy of Sciences, Prague, Czech Republic

S. Banáš
Tesla Trimex, Rožnov p. Radhoštěm, Czech Republic

V. Kohlová and J. Valenta
Faculty of Mathematics and Physics, Charles University, Prague, Czech Republic

I. Pelant
Institute of Physics, Czech Academy of Sciences, Prague, Czech Republic
(Received 16 November 1995)

We report on a detailed study of the dynamics of photoexcited carriers in red-emitting porous silicon at room temperature after excitation by 532-nm picosecond laser pulses. Experimental techniques of time-resolved absorption (pump and probe) and photoluminescence are used to cover a very large time interval 10^{-11}–10^{-4} s. The dynamics exhibits fast and slow components. The fast component ($\sim 10^{-10}$ s) is interpreted as a bimolecular recombination of free carriers in the core of nanometer-sized silicon nanocrystallites, and the slow component ($\sim 10^{-4}$ s) originates in the recombination of carriers rapidly trapped in the surface localized states. We propose a rate-equation model which enables us to describe well the complete photoexcited-carrier dynamics from picoseconds to hundreds of microseconds. Our results strongly support the key role of localized states on the surface of a Si network in the steady-state red photoluminescence of porous silicon. [S0163-1829(96)01935-2]

I. INTRODUCTION

The demonstration of the efficient photoluminescence of porous silicon (PS) at room temperature reported five years ago[1] started an intense activity in the investigation of microscopic properties of this material with application viewpoints in the fabrication of efficient electroluminescent devices based on PS. However, many fundamental questions have not been answered yet. Various models describing optical properties of PS have been considered, but none of them can describe all experimental results well. In particular, luminescence mechanisms have not yet been identified. From both fundamental and application viewpoints, a study of the dynamics of photoexcited carriers is of great importance.

Many studies were devoted to photoluminescence (PL) dynamics in PS,[2–10] and large scales of decay times and decay behaviors were reported. It should be stressed that we are dealing only with red-emitting PS in this paper. We shall not discuss the case of the so-called rapid-thermal-oxidized PS where an intense fast blue PL component has been observed.[11,12] Most of the studies agree about finding a comparatively slow red PL decay dynamics at room temperature. Therefore, most of the studies concentrate on the microsecond time scale.[7–10] Only a few papers pay attention to the initial stage of dynamical behavior, which takes place during and/or immediately after excitation of the PS sample by sufficiently short light pulses studied by picosecond PL (Refs. 2–5) or absorption picosecond[13–16] and femtosecond[6] spectroscopy techniques. In this paper, we report on a detailed study of the room-temperature dynamics of photoexcited carriers in luminescent PS on a very large time interval (10^{-11}–10^{-4} s) using the experimental techniques of time-resolved absorption (picosecond time scale) and photoluminescence (picoseconds to hundreds of microseconds). We clearly distinguish two components in the dynamics. The fast component decays on a time scale of hundreds of picoseconds, while the slow one extends up to hundreds of microseconds. We propose a model that describes well, for the first time to our knowledge, the complete PL dynamics. Our model strongly supports the key role of localized states on the surface of the Si network in the steady-state red PL in PS.

The paper is organized as follows. In Sec. II, the experimental techniques and sample preparation are described. The experimental results and the relevant rate-equation model are presented in Sec. III. The fast and slow components of the carrier dynamics are discussed separately. The conclusions are given in Sec. IV.

II. EXPERIMENT

A. Measurement techniques

The dynamics of PL excited by 532-nm pump pulses was measured using a single-shot streak camera (IMACON 500, J. Hadland, time resolution of ~3 ps). The dynamics of the differential absorption was measured by standard pump and probe technique. The pump pulses were obtained, as in the

0163-1829/96/54(11)/7929(8)/$10.00 © 1996 The American Physical Society

above case of PL dynamics, by frequency doubling of the 1064-nm Nd:YAG (yttrium aluminum garnet) laser output in a KDP crystal (532 nm, 33 ps, energy ≈100 mJ/cm^2). The tunable probe pulses (532–1064 nm, ~40 ps, energy <0.1 mJ/cm^2) were spectrally selected from a picosecond continuum. The diameters of the pump and the probe beams were 0.5 and 0.05 mm, respectively. The time delay between the pump and probe pulses was varied using an optical delay line. The beams were polarized orthogonally to each other, but the results of our measurements did not depend on the polarization directions. The probe pulse monitors the transmission T_E (T_0) of the sample after (without) the pump. It is connected with the relevant absorbancies A_E (A_0) as $T_{E,0}=\exp(-A_{E,0})$. The differential absorbance A_D is given as $A_D=A_E-A_0$.

The dynamics of PL on time scales longer than tens of nanoseconds was measured by dispersing the luminescent light by a monochromator, and detecting it using a photomultiplier and an oscilloscope. The time resolution of this setup was ~15 ns.

Auxiliary measurements to characterize the samples were also performed. cw PL was excited by a 488-nm line from an Ar-ion laser and monitored by an OMA 2 optical multichannel analyzer. The spectra were corrected for the spectral response of the apparatus. The conventional transmission spectra were measured by a standard double-beam spectrophotometer. All experiments were performed at room temperature.

B. Samples

Both PS samples attached to a c-Si substrate and self-supporting PS membranes have been used throughout this study. P-type 1–10-Ω cm Si wafers were the starting material for the preparation of PS by conventional electrochemical anodization. The self-supporting membranes were prepared by anodization of the substrate in HF acid solution ($HF:H_2O=3:1$) with current densities 30–50 mA cm^{-2}. The thickness of the samples was ~25 μm. To facilitate the PL and pump and probe experiments, the membranes were clamped between two quartz slides. The samples attached to the substrate were electrochemically anodized in a HF acid-ethanol solution (50% HF:ethanol=1:1). Two sets of samples were prepared. The samples of the first set (labeled set II) (1.3-Ω cm wafers) were anodized with the current density of 10 mA/cm^2 for 10–40 min, those of the second set (labeled set V) (0.9-Ω cm wafers) were anodized with the current densities 10–50 mA/cm^3 for 5 min. An example of conventional absorption and photoluminescence spectra of a self-supporting PS sample is shown in Fig. 1.

III. RESULTS AND DISCUSSION

Two components can be distinguished in the dynamics of both the PL and transient absorption as measured by picosecond and slower techniques. The fast component has a decay of the order of 100 picoseconds, while the slow component decays longer, up to hundreds of microseconds. In what follows, we demonstrate that the two components are of different origin, due to recombination of carriers in two distinct energy states, as suggested by their different spectral and intensity behaviors described below. We have already suggested[16] the assignment of the two components as follows: the fast one is due to the recombination of photoexcited carriers in the core of silicon nanocrystals, while the slow component is connected to the recombination of carriers localized in surface states. We will discuss the two components separately.

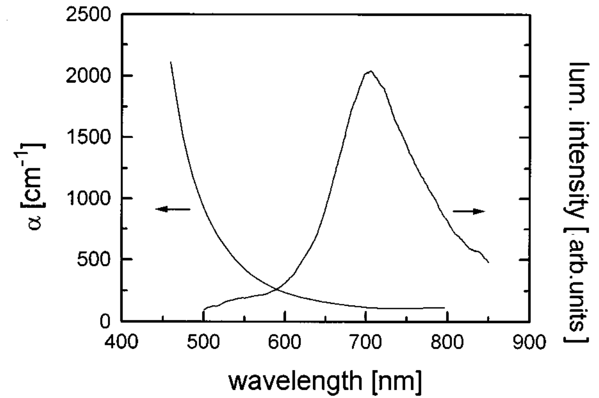

FIG. 1. Typical absorption and luminescence spectrum of the self-supporting PS sample studied. (The absorption coefficient is not corrected for Fresnel losses, and the PL spectrum is obtained with a 488-nm cw excitation).

A. Fast component (picosecond dynamics)

First we studied carrier dynamics in PS using picosecond spectroscopy techniques. The dynamics of differential absorbance A_D at wavelength of 1064 nm of the self-supporting PS sample from Fig. 1 is shown in Fig. 2(a). In Fig. 2(b) the dynamics of spectrally integrated PL of the same sample is shown. In both cases the sample was excited by a 532-nm picosecond pulse. The dynamics of both differential absorbance and PL follow the same time course, i.e., the transmission and emission measurements monitor identical excited states (the apparent difference is due to different time resolution of both techniques of measurement).

The data shown in Fig. 2(a) indicate an induced absorption, i.e., a positive differential absorbance A_D which decays in time. A positive A_D is connected with the excited-state absorption. On the other hand, the excitation of carriers across the gap changes the occupancy of the upper and lower states, which leads to the bleaching of the absorption (a negative A_D). In crystalline direct-gap bulk semiconductors, the bleaching of the ground-state absorption dominates for above-gap wavelengths and $A_D<0$ results. In our case, differential absorbance A_D is positive for all wavelengths in the interval 532–1064 nm. This is also illustrated in Fig. 3, where the result of pump and probe measurement is shown for pump and probe wavelengths of 532 nm. A positive differential absorbance measured by femtosecond pulses was also reported recently by Fauchet.[6]

A positive differential absorbance means that the excited-state absorption is stronger than the interband absorption. This is typical of indirect-gap semiconductors at photon energies slightly greater than the gap energy [e.g., in c-Si (Ref. 17)]. A positive differential absorbance has also been reported in amorphous semiconductors, where it is understood to be mainly due to the loss of k-vector conservation by

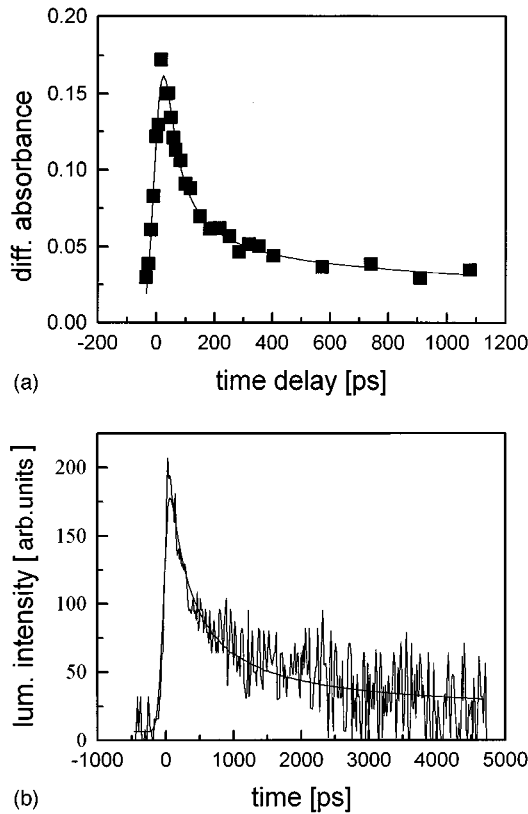

FIG. 2. Dynamics of differential absorbance at 1064 nm (a), and the spectrally integrated PL (b) of a self-supporting PS sample excited by a 532-nm, 33-ps pulse. Solid curves are the best fits using the model proposed [Eqs. (1)–(7); see the text].

disorder [e.g., in a-Si (Ref. 18)]. The same argument is very likely to apply in PS due to its morphology.[19]

In the dynamics shown in Figs. 1–3, two components can be distinguished. The fast component has a decay on the order of 100 picoseconds. The detailed shape of the slow component cannot be obtained from picosecond measurements. In fact, it displays a microsecond decay, as discussed in Sec. III B. The relative weight of the fast and slow components is sample dependent, in some samples the slow component is very weak.

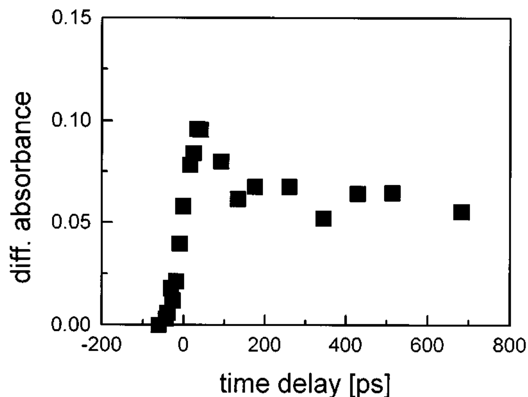

FIG. 3. Dynamics of the differential absorbance at 532 nm of a self-supporting PS sample excited by a 532-nm, 33-ps pulse.

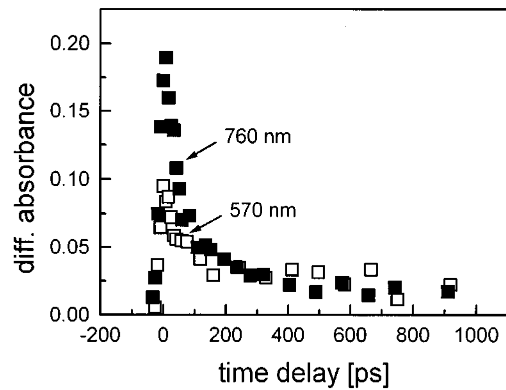

FIG. 4. Dynamics of differential absorbance at 570 and 760 nm for a self-supporting PS sample excited by a 532-nm, 33-ps pulse.

The two components can be separated by their spectral behaviors. In Fig. 4, the dynamics of the differential absorbance at wavelengths of 570 and 760 nm are shown (with a pump pulse wavelength of 532 nm). Clearly, at short-time delays the magnitudes of both dynamics differ considerably, while their slow components are of the same amplitude. This behavior is also illustrated in Fig. 5, where the spectral dependence of A_D is shown for short- and long-time delays. In addition, their behavior with the pump intensity is different, as shown in Fig. 6. The slow component shows saturation. From these results, we conclude that the fast and slow components have different origins, i.e., they are connected with two different types of carriers.

We have previously suggested[16] an assignment of the two components as follows: the fast one is due to a recombination of photoexcited carriers in silicon nanocrystals, and the slow component is connected with the recombination of carriers localized in surface states. The latter interpretation is suggested by the fact that the slow dynamics is affected substantially by the fabrication conditions of PS (see below), and by the observed saturation which indicates a limited number of relevant states.

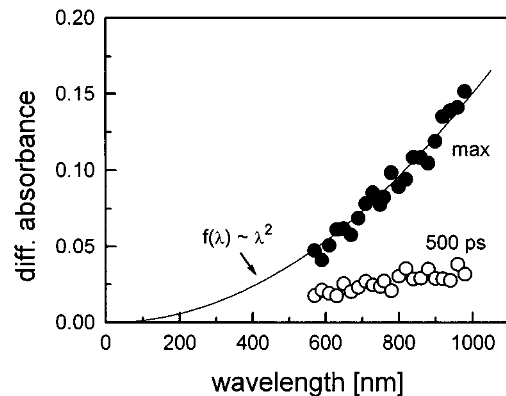

FIG. 5. Spectral behavior of the fast and slow components of the dynamics of differential absorbance (self-supporting PS sample, 532-nm pump pulse). Full circles: fast component, i.e., $A_D(\mathrm{max})-A_D(500\ \mathrm{ps})$. Open circles: slow component, i.e., $A_D(500\ \mathrm{ps})$. The solid curve is a function $f(\lambda)\sim\lambda^2$ corresponding to the Drude model of free-carrier absorption.

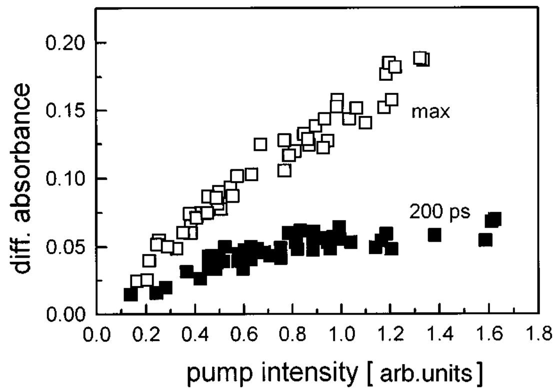

FIG. 6. Intensity behavior of the fast and slow components of the dynamics of differential absorbance. (Self-supporting PS sample, 532-nm pump pulse). Differential absorbance at maximum (open squares) and at a time delay of 200 ps (full squares) vs the pump pulse energy.

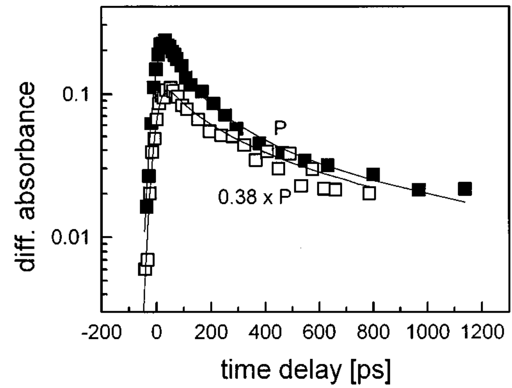

FIG. 7. Dynamics of the differential absorbance at 1064 nm, of a self-supporting PS sample excited by a 532-nm pulse at two different pump pulse energies. The solid curve for P is the best fit according to the model proposed with no apparent slow component [$p=0$, Eqs. (1)–(6); see text]. The solid curve for $0.38P$ is computed without any adjustable parameters using the best-fit values of $B=4\times10^{-10}$ cm^3 s^{-1} and $\sigma=9\times10^{-18}$ cm^2.

In connection with an interpretation of the slow component, thermal effects might be considered. However, in the present case the pure thermal origin of the slow component can be ruled out. Indeed, we can see the same shape of dynamics in both the photoluminescence and transient absorbance measurements [see Figs. 2(a) and 2(b)]. Moreover, an estimate of the peak rise in temperature can be calculated using the specific-heat capacity and density of c-Si for silicon nanocrystals, and the density of photoexcited carriers in silicon nanocrystals ($\lesssim10^{20}$ cm^{-3} in our experiments). The maximum temperature rise is ~20 K. This corresponds to the ~5-meV shift in the band-gap energy, which means a ~1–3 % increase in the absorption at the pump wavelength. However, the positive absorbance is due to the excited-state absorption, the temperature dependence of which is very weak. We have verified that by direct measurement of the dynamics of differential absorbance, with the result that neither its shape nor amplitude depend on the sample temperature in the interval 295–390 K.

The conventional absorption (see Fig. 1) in the spectral interval of Fig. 5 is rather small, so that the negative contribution to the differential absorbance is supposed to be negligible—at least for wavelengths greater than 700 nm. That is why the spectral shape of A_D should be given by the spectral dependence of the excited-carrier absorption. The simple description of free-carrier absorption by the Drude model gives the free-carrier–absorption cross-section $\sigma(\lambda)\sim\lambda^2$. Indeed, the data in Fig. 5 (short time delays) seem to follow this function plotted as a solid curve. This suggests that the transient absorption observed shortly after photoexcitation is due to carriers in the extended states of silicon nanocrystals. The λ^2 behavior of the transient absorption was also reported very recently also by Fauchet[6] and Grivickas and Linnros.[20]

The fast initial decay depends on the photoexcited carrier density. This is illustrated in Fig. 7, where the dynamics of differential absorbance is shown at two pump pulse intensities for the sample showing no apparent slow component in the differential absorbance dynamics. In Fig. 8, the value of the differential absorbance at the time delay of 30 ps is plotted versus the pump pulse energy fluence. The data in Figs. 7 and 8 clearly suggest a nonlinear behavior of the decay.

What type of nonlinearity is this? We have recently proposed a rate-equation model involving a bimolecular recombination to describe the picosecond dynamics of photoexcited carriers.[15] Here we present a more detailed treatment stressing the spatiotemporal formulation of the problem. The photoexcited carrier density $N(z,t)$ in the core of nanocrystals can be described by the following rate equation:

$$\partial N(z,t)/\partial t = P(z,t) - BN(z,t)^2, \quad (1)$$

where z is a coordinate in the direction of the propagation of light, $P(z,t)$ is the pumping, and B is a coefficient of the bimolecular recombination. In general, the sample thickness

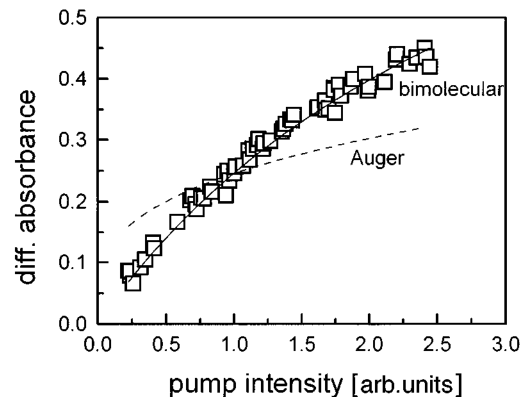

FIG. 8. Differential absorbance (at 1064 nm, self-supporting PS sample, 532-nm pump) at a time delay of 30 ps vs excitation. Squares: experimental points. The solid curve is computed [model of bimolecular recombination, $p=0$, Eqs. (1)–(6)] without any adjustable parameters using the values of B and σ from Fig. 7. The dashed curve is computed using the model of Eqs. (1)–(6), where bimolecular recombination is replaced by Auger recombination $\sim CN^3$ with parameters obtained from the best fit for $P=1$ (see text). Auger constant $C\approx10^{-29}$ cm^6 s^{-1}.

L is larger than the absorption length of the pump pulse, which leads to an inhomogeneous excitation profile (in the z direction). We do not take into account the transversal effects. The pumping $P(z,t)$ can be expressed as

$$P(z,t)=\alpha_0(1-p)I(z,t)/h\nu, \quad (2)$$

where the saturation of the absorption is neglected. Here α_0 is the small signal absorption coefficient of the sample, and $I(z,t)$ is the pump pulse profile. Parameter p gives the fraction of carriers which are transferred to the localized states, where they recombine on a microsecond time scale. The trapping of carriers is supposed to be very fast in this model. This is in accord with results of subpicosecond measurements showing that trapping of carriers is a femtosecond process.[6] If we neglect its decay for times $\lesssim 1$ ns, the density $n(z,t)$ of the trapped carriers can be described as

$$n(z,t)=p\alpha_0\int_{-\infty}^{t}(I(z,t')/h\nu)dt'. \quad (3)$$

The absorption coefficient of the sample is then

$$\alpha(z,t)=\alpha_0+\sigma N(z,t)+\sigma_1 n(z,t), \quad (4)$$

where σ is the free-carrier absorption cross section, and σ_1 is the absorption cross section connected with localized carriers. In general, α_0, σ, and σ_1 are spectrally dependent, and so is the absorption cross section α. That is why the absorption of the sample is different for the pump and for the probe pulses in the two-color pump and probe experiment. The transport equation for the pump intensity can be written

$$\partial I(z,t)/\partial z=-\alpha(z,t)I(z,t). \quad (5)$$

We approximate laser pulses by a temporal Gaussian function; their magnitudes are known from the experiment. The differential absorbance of the sample of thickness L can be written as

$$A_D(t)=\int_0^L\left[\sigma N(z,t)+\sigma_1 p\int_{-\infty}^{t}(\alpha_0 I(z,t')/h\nu)dt'\right]dz. \quad (6)$$

We solve the above equations numerically, and convolute the differential absorbance with the Gaussian probe pulse to model the absorption experimental data. From our previous measurements,[15,16] $B=4\times10^{-10}$ cm^3 s^{-1}. We can fit the experimental curves $A_D=A_D(t)$ at any wavelength with $(\sigma_1 p)$ and σ as fitting parameters. The best fits, shown as the solid curves in Figs. 2 and 7, are obtained for $\sigma=2\times10^{-18}$ and 9×10^{-18} cm^2, respectively. These values of σ should be compared to the values reported previously in PS (Ref. 20) (5×10^{-18} cm^2 at 1.3 μm), c-silicon[17] (5×10^{-18} cm^2 at 1064 nm), and amorphous silicon[18] (3×10^{-18} cm^2 at 1064 nm). The dynamics in Fig. 7 is fitted well with $p=0$, which shows that the weight of the slow component is rather small for this particular sample. Integrating the above equations up to 30 ps for various pump pulse energies gives an excellent agreement with the experimental points in Fig. 8 (full curve) without any adjustable parameters. This again supports the bimolecular feature of the recombination. The three-particle Auger nonradiative recombination was suggested by some authors to interpret their data.[20,21] Our experimental data cannot be fitted only by the standard Auger ($\sim N^3$) kinetics, which does not seem to reproduce correctly either the shape of decay curves or the intensity dependences. For comparison, we show the Auger intensity dependence as a dotted curve in Fig. 8. This was obtained by fitting the decay curve of Fig. 7 [using a modified model in which the recombination term $\sim N^2$ of Eq. (1) was replaced by the term $\sim N^3$] for $P=1$, and by solving the relevant rate equations with the best-fit values of parameters (the fit—not shown here—is of bad quality, not reproducing the experimental decay profile correctly, and the value of Auger recombination constant has to be taken at least two orders of magnitude larger then that of c silicon for pump rates corresponding to the experiment).

The value of the bimolecular recombination coefficient B is found to be of the same order as that of radiative recombination in direct-gap semiconductors [e.g., $B=2\times10^{-10}$ cm^3 s^{-1} in GaAs,[22,23] $B=2.4\times10^{-10}$ cm^3 s^{-1} in GaSb (Ref. 24)]. The value of this coefficient in indirect semiconductors is several orders of magnitude smaller [e.g., $B=5.4\times10^{-14}$ cm^3 s^{-1} in GaP and $B=1.8\times10^{-15}$ cm^3 s^{-1} in c-Si (Ref. 24)]. The bimolecular recombination with coefficient of the same order[25,26] ($B=7\times10^{-10}$ cm^3 s^{-1}) or slightly larger[27] ($B=7\times10^{9}$ cm^3 s^{-1}) has also been reported in amorphous silicon, where it was interpreted as a nonradiative Auger-like process. Its bimolecular character is explained by an Auger recombination of two free charge carriers and one trapped charge carrier,[25,26] or by an Auger recombination of highly correlated electron-hole pairs.[27]

B. Slow component (microsecond dynamics)

Before we proceed to the description of the slow PL dynamics studied by a photomultiplier, let us mention how the fast and the slow components superpose in the PL decay as measured by the streak camera (time interval $\lesssim 15$ ns). The fast (picosecond) PL decay can be observed for $\lambda \lesssim 650$ nm for 532-nm pumping. In accord with the above discussion, it can be understood as a contribution due to the carriers in the extended states in the core of nanocrystals. The slow PL component $I_{SE}(t)$, which is due to the localized carriers, decays on a microsecond time scale (as discussed below). Using the above rate equations, PL intensity can be then fitted by an expression

$$I(t)=KN(t)^2+I_{SE}(t). \quad (7)$$

Here $I_{SE}(t)$ can be approximated as $I_{SE}(t)\approx I_0$ for times greater than the pulse duration and smaller than 10 ns, so that the experimental constant K and I_0 are the only fitting parameters. In Eq. (7), $N(t)$ is an average value of carrier density taken over the absorption length of the sample. The fits are of very good quality, as illustrated in Fig. 2(b), where the best fit is shown as a solid curve. This means that we monitor the states—both free carriers and localized states—which are connected with both the luminescence and absorption. In general, $B=B_{rad}+B_{nonrad}$. However, a fairly strong fast luminescence suggests that the bimolecular recombination is rather a radiative process. For the slow component, the luminescence efficiencies and absorption cross sections in luminescence and absorption data, respectively, are connected with the density of localized carriers in our model. This

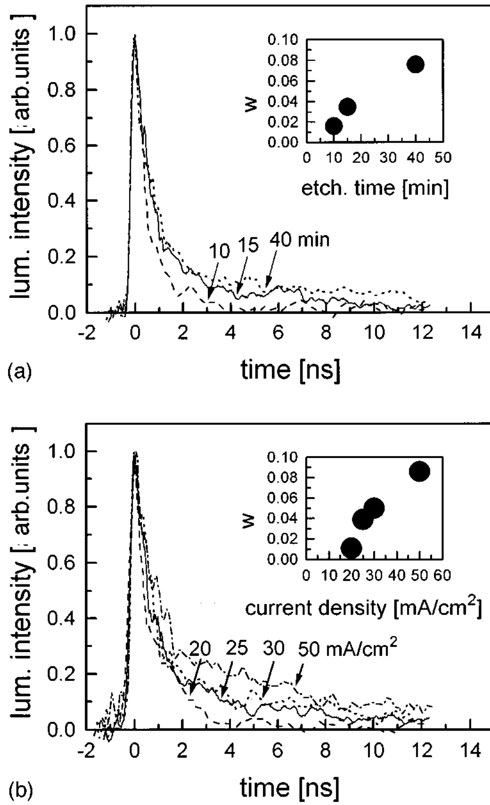

FIG. 9. PL dynamics of samples of PS on a substrate. (a) Set II, anodization times 10, 15, and 40 min. (b) Set V, anodization current density 20, 25, 30, and 50 mA/cm^2. Curves are normalized. Insets: relative weight w of the slow component vs anodization time (a) and current density (b).

makes it apparently impossible to find the relative importance of the radiative and nonradiative processes in the slow-carrier recombination.

To confirm the different origin of the fast and slow components, we have studied the influence of anodization conditions on carrier dynamics. In particular, we have measured PL dynamics for two sets of samples described above. The results for the sets II and V are shown in Figs. 9(a) and 9(b), respectively. Clearly the relative weight of the slow component increases with both anodization time (for constant anodization current) and anodization current (for constant anodization time). This can be clearly seen in the insets, showing the relative weight of the slow component w versus the anodization time [Fig. 9(a)] or the anodization current [Fig. 9(b)]. w is obtained as the ratio of the intensity of the slow component I_0 (defined above) to the total intensity at the maximum. To understand these observations, we recall that it has been shown[28] for lightly doped Si substrates ($\sim$1 Ω cm) that the increase of both the anodization time and anodization current density leads to higher porosity and, consequently, to the decrease of specific surface area for porosities >50%. This means that in both cases the dimensions of Si nanoparticles become smaller and, therefore, the relative importance of their surface states rises. This is in agreement with the increase of w presented in Fig. 9, which strongly supports the assignment of the PL slow component as due to the recombination via localized surface states.

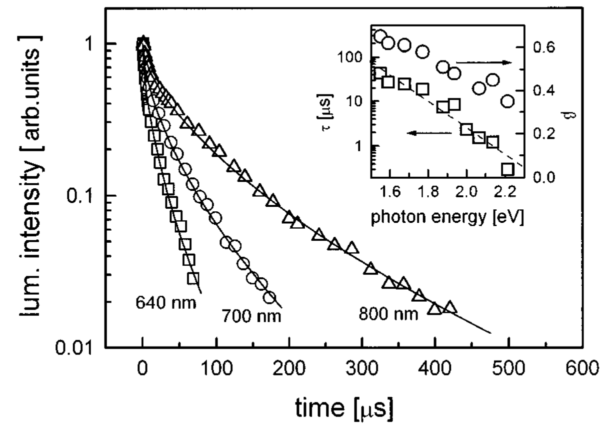

FIG. 10. Spectrally resolved microsecond PL delay (sample of PS on substrate anodized for 40 min, set II). Solid curves are the best fits using Eq. (8). Inset: parameters β and τ of function (8) vs the PL photon energy.

The study of PL dynamics on a longer time scale using a photomultiplier and an oscilloscope has shown that for all the samples the slow component decays on a microsecond time scale, that it is nonexponential, and that it is faster at shorter wavelengths. As an example, the slow part of the PL decay for the sample anodized for 40 min (set II) is shown in Fig. 10. Its profile follows the stretched-exponential decay law

$$I_{\mathrm{SE}}(t)=I_0\exp[-(t/\tau)^{\beta}], \tag{8}$$

as already proposed by other groups.[7–10] In this function, the parameter β is $0\leqslant\beta\leqslant1$. The values of the time constant τ lie in the interval 1 μs–1 ms for the samples studied. This function indicates a dispersive diffusion of photoexcited carriers, most probably within a single nanocrystal.[29] Under the conditions of our experiments the so-called hopping mechanism applies,[8] and parameter β is given by the geometry of localized states. The fits of the experimental data by Eq. (8) have very good quality (the solid curves in Fig. 10), and they provide values for fitting the parameters β and τ which are shown in the inset of Fig. 10. τ is shown to be linear in the semilog plot versus PL photon energy E, which suggests that it follows approximately an exponential function, $\tau\sim\exp(-\Gamma E)$, the value[30] of $\Gamma\sim6$ eV^{-1} being the same for all the samples of sets II and V. The exponential behavior was also observed by others,[7–10,31] and interpreted as due to the exponential distribution of localized states within the band gap.[31] The value of Γ we have obtained agrees well with other published data.[8,10] Parameter β (see the inset of Fig. 10) has been found to be a slowly decreasing function of luminescence photon energy, which is in very good agreement with both the data and theoretical calculations published.[8,10] The behavior of β is similar for all samples measured.

The decay function Eq. (8) can be understood as a consequence of distribution $g(\lambda)$ of the decay rates λ of nonradiative processes which are supposed to dominate the decay,[10] so that

$$I(t)\sim\int_0^{\infty}g(\lambda)\exp(-\lambda t)d\lambda. \tag{9}$$

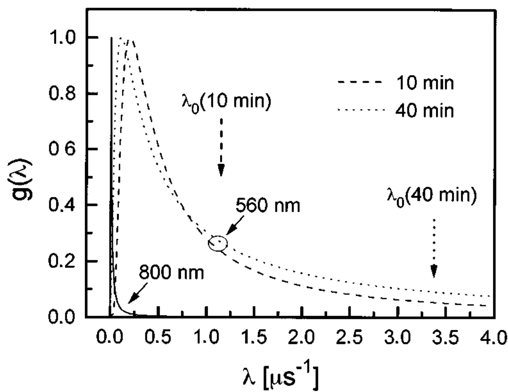

FIG. 11. Distribution function $g(\lambda)$ for two samples of PS of set II (anodized for 10 and 40 min) at PL wavelengths of 800 and 560 nm. Both curves overlap in the case of 800 nm. The average values of the decay rate λ_0 for 560 nm are shown by arrows.

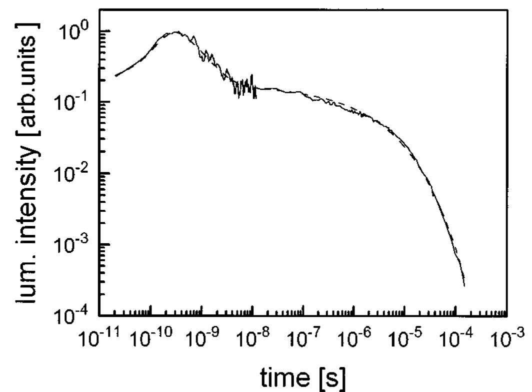

FIG. 12. PL dynamics of a PS sample (set II, 40-min anodization time) in a broad time interval. The dashed curve is the best fit according to the model proposed.

By inverse Laplace transform of Eq. (9), the distribution function $g(\lambda)$ can be found. In Fig. 11, the distribution functions for two samples of set II (10- and 40-min anodization times) are shown. The distribution functions for 800-nm PL overlap for both samples. The values of the average decay rates λ_0 corresponding to the 560-nm distribution functions are shown by arrows in Fig. 11. It can be seen that, at higher photon energies, the distribution $g(\lambda)$ is broader and the decay faster, and at lower energies the narrower distribution and slower decay are typical. This can be understood in terms of the greater number of opportunities for relaxation for carriers in high-energy states in the band tail. The anodization conditions modify the functions $g(\lambda)$. Longer anodization times mean faster decay at high photon energies (see Fig. 11). This can be interpreted as an increase in the density of relevant energy states, as suggested previously,[32] which means that morphology and/or surface chemistry are affected.

The simultaneous measurement of PL dynamics using a steak camera and photomultiplier gives a complex picture of PL decay in the time range of six orders of magnitude. As an example, PL dynamics of the sample anodized for 40 min (set II) is shown in Fig. 12. The dashed curve which reproduces the experimental data well, is obtained using the proposed model [Eqs. (1), (7), and (8)] with the values of constants given above.

IV. CONCLUSION

We have investigated the dynamics of photoexcited carriers in PS after excitation by picosecond 532-nm laser pulses at room temperature. The dynamics exhibits fast and slow components. We have suggested a rate-equation model which makes it possible to fit well the observed carrier dynamics in a large time interval of 10^{-11}–10^{-4} s. The fast component is believed to be due to a bimolecular (both radiative and nonradiative) recombination of carriers in the core of the nanometer-sized silicon crystallites. The standard (trimolecular) nonradiative Auger recombination process seems to be of much less importance in PS under our experimental conditions. We interpret the slow component as a recombination of carriers rapidly trapped in states localized at the surface of Si crystallites. This recombination occurs simultaneously with the carrier hopping relaxation process through the tail states. The above interpretation is consistent with the observed fact that the increasing anodization time, as well as the increasing anodization current, entails a higher weight of the slow component as a consequence of the enhancement of the relative importance of the surface states. Our results strongly support the model in which steady-state PL is related to radiative recombination from localized states on the surface of Si nanocrystallites.[33]

ACKNOWLEDGMENTS

This work was supported in part by the EC Grant Nos. PECO 7839 and ERB CHRX CT 93 0133, by a grant from the Grant Agency of Czech Republic 202/93/0383, by Charles University Grant No. 287, and by Grant No. A1010528 of the Grant Agency of the Czech Academy of Sciences. We thank Professor M. Stutzmann and Dr. J. Kočka for valuable discussions.

[1] T. L. Canham, J. Appl. Phys. **57**, 1046 (1990).
[2] T. Matsumoto, T. Futagi, H. Mimura, and Y. Kanemitsu, Phys. Rev. B **47**, 13 876 (1992).
[3] T. Miyoshi, K. S. Lee, and Y. Ayagi, Jpn. J. Appl. Phys. **31**, 2470 (1992).
[4] Y. Kanemitsu, T. Matsumoto, T. Futagi, and H. Mimura, Jpn. J. Appl. Phys. **32**, 411 (1993).
[5] J. Wang, W. Wang, J. Zheng, F. Zheng, X. Hou, X. Wang, H. Wang, and X. Zheng, Solid State Commun. **91**, 239 (1994).
[6] P. M. Fauchet, in *Microcrystalline and Nanocrystalline Semiconductors*, edited by L. Brus, M. Hirose, R. W. Collins, F. Koch, and C. C. Tsai, MRS Symposia Proceedings No. 358 (Materials Research Society, Pittsburgh, 1995), p. 525.
[7] X. Chen, B. Henderson, and K. P. O'Donnell, Appl. Phys. Lett. **60**, 2672 (1992).
[8] L. Pavesi, M. Ceschini, and H. E. Roman, Thin Solid Films **255**, 67 (1995).
[9] E. Bustarret, I. Mihalescu, M. Ligeon, R. Romestain, J. C. Vial,

and F. Madeore, J. Lumin. **57**, 105 (1993).

[10] N. Ookubo, N. Hamada, and S. Sawada, Solid State Commun. **92**, 369 (1994).

[11] L. Tsybeskov, Ju. V.Vandyshev, and P. M. Fauchet, Phys. Rev. B **49**, 7821 (1994).

[12] V. Petrova-Koch, T. Muschik, D. I. Kovalev, F. Koch, and V. Lehmann, in *Microcrystalline Semiconductors: Materials Science & Devices,* edited by P. M. Fauchet, C. C. Tsai, L. T. Canham, I. Shimuzu, and Y. Aoyagi, MRS Symposia Proceedings No. 283 (Materials Research Society, Pittsburgh, 1993), p. 179.

[13] T. Matsumoto, N. Hasegawa, T. Tamaki, K. Ueda, T. Futagi, H. Mimura, and Y. Kanemitsu, J. Non-Cryst. Solids **164-66**, 953 (1993).

[14] V. I. Klimov, V. S. Dneprovskii, and V. A. Karavanskii, Appl. Phys. Lett. **64**, 2691 (1994).

[15] P. Malý, F. Trojánek, A. Hospodková, V. Kohlová, and I. Pelant, Solid State Commun. **89**, 709 (1994).

[16] F. Trojánek, P. Malý, I. Pelant, A. Hospodková, V. Kohlová, and J. Valenta, Thin Solid Films **255**, 77 (1995).

[17] H. J. Eichler, T. Brand, M. Glotz, and B. Smandek, Phys. Status Solidi B **150**, 705 (1988).

[18] Z. Vardeny and J. Tauc, Phys. Rev. Lett. **46**, 901 (1973).

[19] M. S. Hybertsen, in *Porous Silicon Science and Technology*, edited by J.-C. Vial and J. Derrien (Springer-Verlag, Berlin, 1995), p. 67.

[20] Grivickas and J. Linnros, in *Microcrystalline and Nanocrystalline Semiconductors* (Ref. 6), p. 543.

[21] I. Mihalcescu, J. C. Vial, A. Bsiesy, F. Muller, R. Romestain, E. Martin, C. Delerue, M. Lannoo, and G. Allan, Phys. Rev. B **51**, 17 605 (1995).

[22] U. Straus and W. W. Rühle, Appl. Phys. Lett. **62**, 55 (1993).

[23] H. C. Case and F. Stern, J. Appl. Phys. **47**, 631 (1976).

[24] M. H. Pilkuhn, in *Handbook of Semiconductors*, edited by T. S. Moss and C. Hilsum (North-Holland, Amsterdam, 1980), Vol. 4, p. 539.

[25] G. Juška, J. Kočka, M. Viliunas, and K. Arlauskas, J. Non-Cryst. Solids **164-166**, 579 (1993).

[26] G. Juška, M. Viliunas, and K. Arlauskas, Phys. Rev. B **51**, 16 668 (1995).

[27] A. Esser, K. Seibert, H. Kurz, G. N. Parsons, C. Wang, B. N. Davidson, G. Lucovsky, and R. J. Nemanich, Phys. Rev. B **41**, 2879 (1990).

[28] A. Halimaoui, in *Porous Silicon Science and Technology* (Ref. 19), p. 33.

[29] A. Kux and M. Ben Chorin, Phys. Rev. B **51**, 17 535 (1995).

[30] J. Kudrna, F. Trojánek, I. Pelant, S. Banáš, V. Kohlová, and P. Malý, Thin Solid Films **276**, 58 (1996).

[31] Y. Kanemitsu, Phys. Rev. B **49**, 16 845 (1994).

[32] T. Miyoshi, K. S. Lee, and Y. Aoyagi, Jpn. J. Appl. Phys. **31**, 2470 (1992).

[33] F. Koch, V. Petrova-Koch, T. Muschik, A. Nikolov, and V. Gavrilenko, in *Microcrystalline Semiconductors: Materials Science & Devices* (Ref. 12), p. 197.